ACS APPLIED MATERIALS & INTERFACES

Research Article

www.acsami.org

Patterned Ni–P Alloy Films Prepared by "Reducing–Discharging" Process and the Hydrophobic Property

Quanyao Yu,[†,‡] Zhixiang Zeng,*[,†] Wenjie Zhao,[†] Yongcun Ma,[†] Xuedong Wu,*[,†] and Qunji Xue[†]

[†]Key Laboratory of Marine Materials and Related Technologies, Zhejiang Key Laboratory of Marine Materials and Protective Technologies, Ningbo Institute of Materials Technology and Engineering, Chinese Academy of Sciences, Ningbo 315201, PR China

[‡]University of Chinese Academy of Sciences, Beijing 100039, PR China

Supporting Information

ABSTRACT: Patterned hydrophobic Ni–P alloy films consisting of orderly and regular micro-nanoscale particles were fabricated through the synergistic effect of electrochemical deposition and chemical deposition. Ni–P alloy films were deposited for different times and characterized by scanning electron microscope (SEM). It was confirmed that the addition of reducing agent induced the formation of nanoscale particles, in contrast with pure Ni film deposited by single electrochemical deposition. As "point-discharge effect", the current density was higher at the edge of the nanoscale particles, and Ni ions would be deposited at the particles through the "point-discharge effect". Then the Ni–P alloy films grew by "reducing–discharging" process. The X-ray photoelectron spectroscopy (XPS) was used to detect the composition and valence states of these alloy films. The existence of oxidation state of element P in these films corresponding to that in $H_2PO_3^-$, also gave direct evidence for the occurrence of chemical deposition, during the electrochemical deposition process. The prolongation of deposition time could provide more time for the patterned morphology to grow up. The surface roughness, evaluated by surface profilometer, increased as the deposition time extension. And these films showed gradually increased hydrophobic properties with the increase in deposition time.

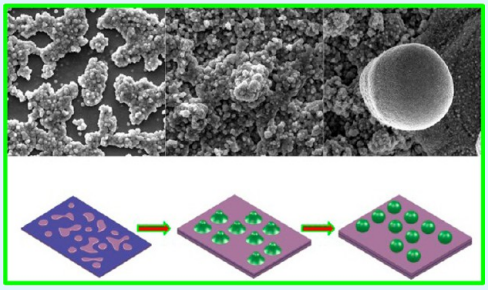

KEYWORDS: *electrodeposition, chemical deposition, synergistic effect, morphology, hydrophobic, patterned surface*

1. INTRODUCTION

Micro-nanostructured patterned films have many applications like superhydrophobicity,[1] sensing,[2] surface Raman enhancement,[3,4] catalysis,[5] optoelectronic,[6,7] and others. In the field of bionics, the superhydrophobic properties of lotus leaves[8] and rose petals[9] are due to their surface morphology with micro-nanoscale structures. In the case of lotus leaves, because of the hierarchical structure, an air cushion existing at the gaps between micro-nanostructures is packaged under the water droplets, making the surface self-cleaning. There are many methods for preparing micro-nanopatterned surfaces, which can be classified into two kinds: top-down[10−12] and bottom-up[13−17] methods. The top-down approach produces micro-nanostructures by deconstructing larger materials with the use of lithographic tools (physical top-down) or through chemical-based processes (chemical top-down[12]). By contrast, the bottom-up approach, micro-nanoscale materials are constructed from atomic or molecular precursors that are allowed to react and grow in size, or self-assemble into more complex structures. The last few decades have witnessed the extensive use of the bottom-up as well as the top-down methods in the fabrication of micro-nanoscale structures.[18,19] Hereinto, the bottom-up nanofabrication method often makes use of deposition techniques (e.g., liquid deposition and vapor deposition) and molecular self-assembly processes (e.g., self-assembled monolayers).

Liquid deposition has been used to fabricate patterned films for many years, as it is low cost, high efficiency, and suitability for large area production. Since Bennett et al. invented electrodeposition of Ni[20] and Brenner and Riddell invented chemical deposition of Ni,[21] Ni films deposited by the two methods have been industrialized for many years. Electrochemical deposition and chemical deposition, as two common liquid depositions, are two traditional approaches used to prepare metallic films and patterned morphologies. And also, both of the deposition approaches are widely used in scientific research in many areas to fabricate micro- and nanomaterials and similar. The electrochemical and chemical fabrication of micro- and nanomaterials has been studied in recent years and many micro-nanomaterials with different crystal habits[22−24] and different morphologies like nanowire,[25] dendritic,[7,26−28] hexagonal,[29] and jellyfish[30] are fabricated successfully. The controlled deposition of nanomaterials is a compelling challenge for modern technology. The possibility of reproducing existing or creating novel devices at the micro-nanoscale is strongly related to the availability of appropriate building tools and the recognition of the growth mechanism of nanomaterials. The identification of growth mechanism of metallic films,

Received: October 17, 2013
Accepted: December 27, 2013
Published: December 27, 2013

dx.doi.org/10.1021/am404590d | ACS Appl. Mater. Interfaces 2014, 6, 1053−1060

especially those with micro-nanostructures, is very helpful for the preparation process and technology. Formation of multiscale surface features is generally attributed to a process called unstable growth. The theory of this process was first discussed for the formation of dendritic structures during thermal solidification by Mullins and Sekerka.[31] This theory was further extended by Aogaki and co-workers to explain formation of multiscale surface features during electrodeposition.[32,33] Most of these models discuss the electrodeposition systems at the limiting condition, which corresponds to the mass transfer limitation of the system. Diffusion mass transfer in the electrolyte favors the growth of the arbitrary protrusions on the deposit surface and enhances the morphological instabilities of the deposit. Recently, copper based multiscale rough surfaces were fabricated through electrodeposition and their hydrophobic properties were intensively studied.[34,35] Furthermore, hierarchical copper based micro-nanostructures were electrochemically deposited under the function of electrochemistry of conducting polymer polypyrrole−polystyrene sulfonate films,[2,36,37] and their performances showed a good sensing property in the sensing of nitrate. Wang and co-workers[4] obtained metal structures with fiber, sheet, cube, yarn-ball, and leaflike morphologies on undoped or doped polyaniline (PANI) membrane employing the tailored conducting polymer chemistry of PANI.

Although the liquid deposition technology has been extensively used, most of the high-quality metal film products are prepared by empirical law in industry. The additive agents' functions, especially some kinds of denier organic additives, have not been known by researchers because of the wide range of deposition reagents and the complex experimental conditions. Although electrochemical deposition and chemical deposition processes of many metal deposition systems are still being studied actively today, most of these give the results based on electrochemical methods. Herein, the two deposition methods were merged into a single deposition solution. The experimental results give quite powerful information to reveal the growth mechanism of patterned alloy films.

Add some reducing agent into the traditional electrochemical deposition cell, the films will be grown up through the two deposition processes. That what will happen to the film structure and the surface morphology is an interesting question to tempt many researchers' appetites. As a simple glimpse to the synergistic effect[38] of our group's previous work (Figure 1), in the electrolyte, Ni ions and electrons could integrate into one unit at the cathode. If this unit does not encounter the reducing agent, the film will grow to be a flat one through single electrodeposition; however, if reducing agent is added into this solution, the film will have a patterned morphology in the end by the synergistic effect of electrodeposition and chemical deposition. These days an overall research has been made to intensively investigate the growth mechanism of these Ni−P alloy patterned films. Herein, the formation mechanism of this superhydrophobic surface is explained in a more acceptable way. The different stages of film growth observed though SEM images and XPS show that the occurrence of electrochemical deposition strongly supports the hypothesis of the synergistic effect of electrochemical deposition and chemical deposition. The alloy film growth by "reducing−discharging" process can give a more clear direction for future work in this research. It is the addition of reducing agent to the solution that induces the formation of nanoscale particles appearing at the surface morphology. The multiscale surface features are formed by the combination of the theory on the unstable growth process. In this work, the electrolyte is kept stirring all the time, which means the diffusion layer is thinner than that without stirring. This makes the deposited particles smaller. This work gives an overall investigation of the variation of patterned morphology to understand the innate character of the formation of patterned films.

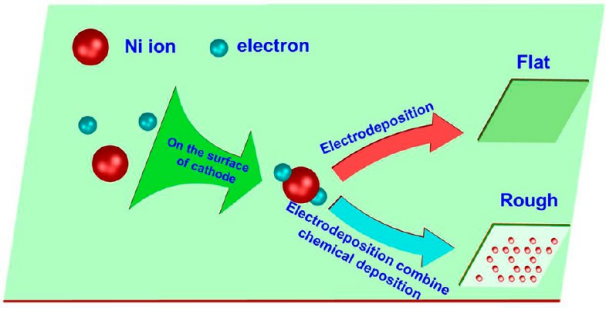

Figure 1. Schematic diagram of the comparison of electrodeposition and synergistic effect of electrochemical deposition and chemical deposition.

2. EXPERIMENTAL SECTION

2.1. Materials and Reagents. Nickel sulfate hexahydrate ($NiSO_4 \cdot 6H_2O$, Sinopharm Chemical Reagent Co. Ltd., CP), citric acid monohydrate (Sinopharm Chemical Reagent Co. Ltd., CP), sodium sulfate anhydrous (Na_2SO_4, Sinopharm Chemical Reagent Co. Ltd., AR), 1,4-butynediol ($C_4H_6O_2$, Aladdin Chemistry Co. Ltd., AR), sodium dodecyl sulfate (SDS, Sinopharm Chemical Reagent Co. Ltd., CP), and sodium hypophosphite (NaH_2PO_2, Aladdin Chemistry Co. Ltd., AR) were used as received. Aqueous solutions were prepared using deionized (DI) water.

2.2. Preparation of Ni−P Alloy Films. The deposition of Ni−P alloy films was carried out at a current density of 15 mA/cm^2 on low alloy steel substrates from electrolytic bath containing 0.125 M $NiSO_4 \cdot 6H_2O$, 0.05 M citric acid, 1.2 g/L SDS, and 0.075 g/L $C_4H_6O_2$. And the concentration of Na_2SO_4 was adjusted to 0.3 M to enhance the electrolyte's ion strength. The pH value of electrolyte was adjusted by adding aqueous ammonia to 5.5. Films with different deposition time (1, 5, 10, 20, 30, and 60 min) were deposited in the solution with 0.05 M NaH_2PO_2. Also, different amounts (0.01, 0.02, 0.03, 0.04, 0.05 M) of NaH_2PO_2 were added to the solution for preparation of Ni−P alloy films with different morphologies. Prior to electrochemical deposition, substrates were activated in a diluted hydrochloric acid (HCl) and subsequently cleaned by DI water. All of the above deposition processes were performed at solution temperature of 70 °C in a two-electrode electrochemical cell with a Ni plate as the anode and low alloy steel substrates as the cathode. During deposition process, the electrolyte was kept stirring with a magnetic stirrer. Pure Ni films with different deposition time were deposited as control experiment. Also, smooth Ni−P alloy film with 0.05 M H_3PO_3 in the pure Ni deposition electrolyte was prepared to test the theoretical contact angle of a smooth Ni−P alloy film. The power station was PSM-3400 (GW, Taiwan, China).

2.3. Ni−P Alloy Film Characterization. Surface morphologies of films were examined by using a scanning electron microscope (SEM, FEI Quanta 250 FEG, US), and films chemical composition and elements mapping are detected by energy dispersive X-ray spectrum (EDX). The microstructures of films were performed by an X-ray diffraction (XRD, Bruker-AXS: D8 Advance, Germany). The valence state of element Ni and P in the films of deposited different time were performed by an X-ray photoelectron spectroscopy (AXIS ULTRADLD, England). The surface roughness was measured by a surface profilometer (Alpha-Step IQ, US). Surface contact angle (CA) was detected by using a contact angle meter (OCA20, Germany).

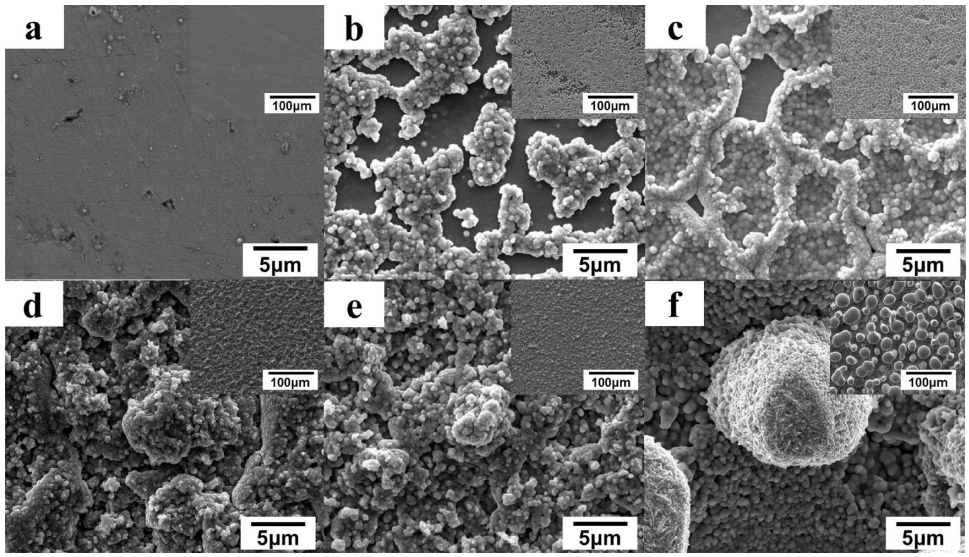

Figure 2. Effect of deposition time on the Ni–P alloy films surface morphologies. SEM images of Ni–P alloy films deposited for (a) 1 min; (b) 5 min; (c) 10 min; (d) 20 min; (e) 30 min; (f) 60 min. Insets are low magnification SEM images.

Water droplets with a volume of 2.0 μL were dropped carefully onto surfaces. Before the contact angle characterization, all films were ultrasonically cleaned in ethanol solution for 10 s to eliminate the unexpected contamination. All the tests were performed at room temperature. The contact angles were tested with samples just after preparation and after storage for 3 months.

3. RESULTS AND DISCUSSION

3.1. Patterned Film Growth and Characterization. Ni–P alloy films are deposited on the low alloy steel substrates polished before use for different deposition times through galvanostatic methods. The SEM images of Ni–P alloy patterned films deposited for different times are shown in Figure 2. As a whole, the film deposited for 1 min (Figure 2a) is smooth, with some nanoscale particles scattering at the film surface. By comparison with the morphology of pure Ni film deposited by single electrochemical deposition for 1 min (Supporting Information Figure SI2b) which is smooth without any nanoscale patterns, these nanoscale particles are caused by the addition of reducing agent according to the single variable theory. From the EDX elements mapping (Supporting Information Figure SI1), elements Ni and P uniformly distributed on the selected area, without any aggregation phenomena appearing at some special places like the particle regions. It means that the film is mainly deposited by the electrochemical deposition, as both elements Ni and P can be reduced to elemental state by the electrons.[39] In this electrolyte, the ratio of element Ni and P is about 2.5, which is very large compared to that of the traditional chemical deposition system (about 0.33).[40] That is to say, the P content is very low in this electrolyte. If there happens some chemical deposition, the chemical composition of deposits may not provide any valuable information. The chemical composition of nanoscale particle areas and flat areas on 1 min deposited Ni–P alloy film do not show any difference (results are not shown). The pure Ni film as control sample deposited for 1 min is also tested by EDS at selected area to state that the black area is not deposited the Ni layer. So, it is clearly shown that pure Ni deposit possesses no nanoscale particles or other special morphology. When the deposition time prolongs up to 5 min (Figure 2b), nanoscale particles formed at the surface of alloy film grow larger, crowd, and agglomerate together, constituting "cluster islands" drifting on the sea of smooth Ni–P alloy film surface. Extending the deposition time to 10 min (Figure 2c), these cluster islands area increase and squeeze each other, leading to the edges of these islands turning up. These islands deposited for 10 min make the film possess higher roughness, and almost cover the no characteristic smooth film. As the deposition continues, the three-dimensional patterned morphology emerges slightly when the deposition time is up to 20 min (Figure 2d) and 30 min (Figure 2e), and the mastoid-like structures shape up when the film is deposited for 1 h (Figure 2f). The pure Ni films deposited by electrochemical deposition for different deposition time are also prepared in this work for comparison (Figure 3). After the Ni films completely cover the substrate (deposition time is longer than 5 min (Figure 3c and d)), the

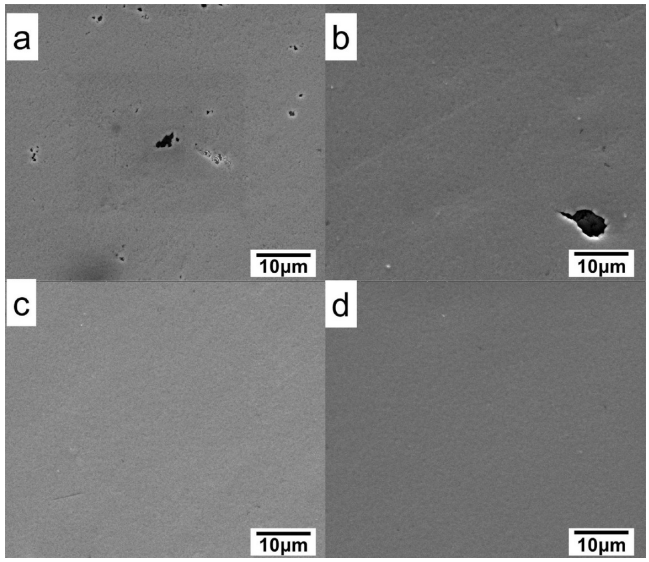

Figure 3. Control samples of pure Ni films. SEM images of pure Ni for different deposition time: (a) 1 min; (b) 5 min; (c) 10 min; (d) 30 min.

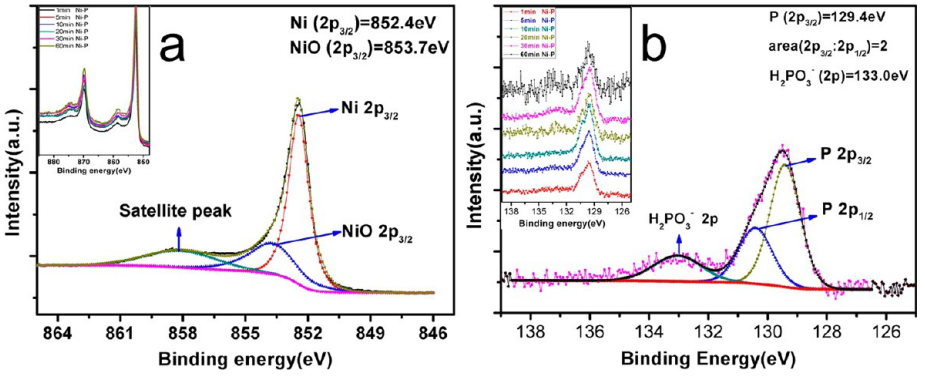

Figure 4. XPS data and fitted curves of elements Ni (a) and P (b) in films deposited at different deposition times. Insets show XPS data of Ni (a) and P (b) samples prepared at different deposition times.

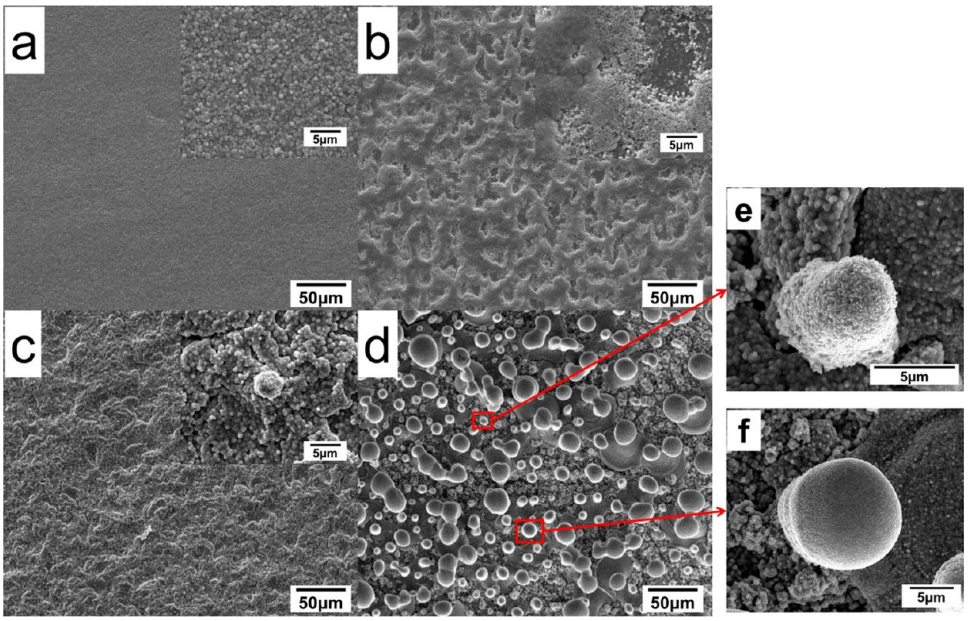

Figure 5. Effect of reducing agent (sodium hypophosphite) content on the surface morphologies of Ni–P alloy films deposited for 60 min. SEM images of Ni–P alloy films deposited with different content of hypophosphite in solutions: (a) 0.01 M; (b) 0.02 M; (c) 0.03 M; (d) 0.04 M. the insets are the enlargements of each film. On the film deposited with 0.04 M hypophosphite in the solution, two single mastoid-like structure regions are selected (e and f) to show the different growth stages on the same sample.

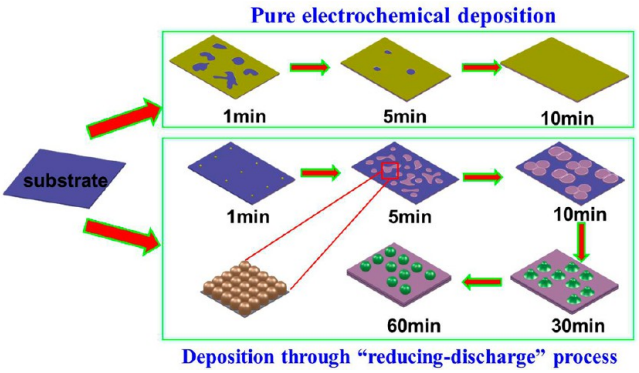

Figure 6. Brief diagram of the mechanism of formation of pure Ni films (above) and Ni–P alloy patterned films (bottom).

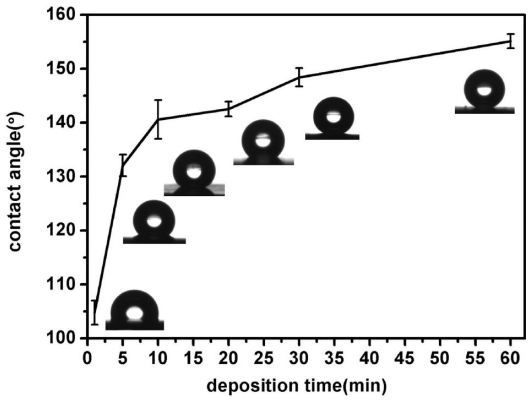

Figure 7. Contact angle variation with the change of deposition time.

pure Ni films are smooth and do not show any feature morphology. These Ni–P alloy films deposited for different times reveal the discipline of film morphology evolution. From the whole range view (insets in Figure 2), these films' morphology is evenly distributed. The growth of schematic diagram is shown in Figure 6.

XRD patterns of these Ni–P alloy films deposited for different time is shown in Figure SI3 (Supporting Information).

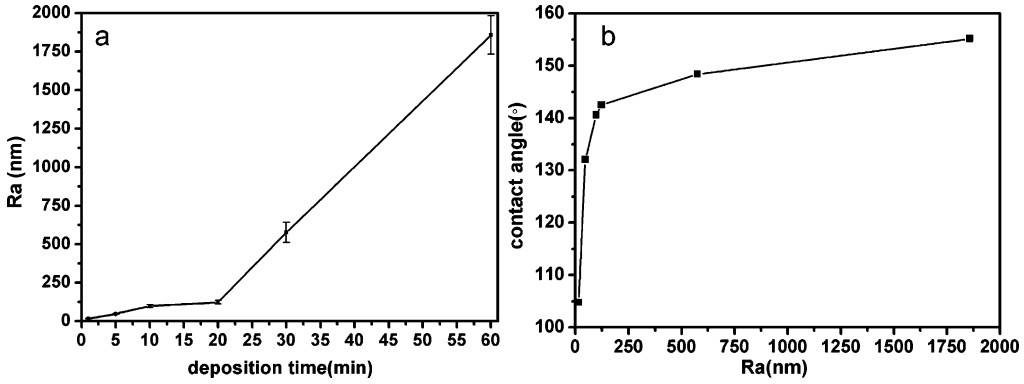

Figure 8. (a) Roughness variation of films vs film deposition time. This curve pattern shows that the surface roughness gradually increases along with the increase of deposition time. This regulation has a good correspondence with the variation of film contact angles with water (b).

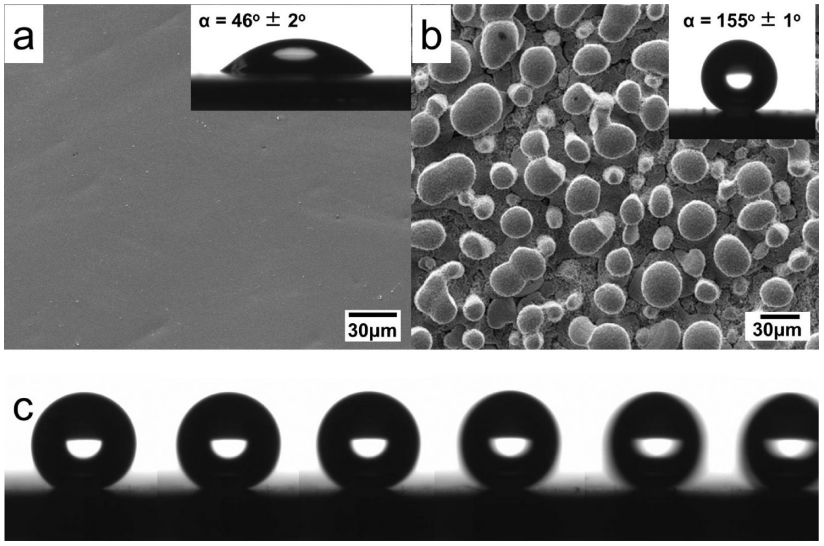

Figure 9. SEM images of (a) Ni–P smooth film and (b) Ni–P patterned films. The insets show the contact angle with water droplets. The Ni–P smooth film shows hydrophilic property with contact angle of 46° ± 2°. Ni–P patterned film shows superhydrophobicity with contact angle of 155° ± 1°. (c) Photographs of a water droplet sliding on the tilt patterned film exhibiting very small contact angle hysteresis.

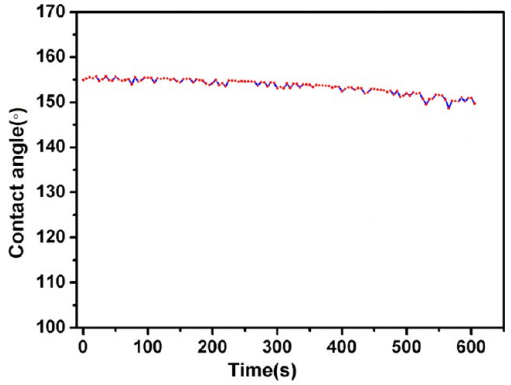

Figure 10. Contact angle variation with the standing time. The CA became smaller with the prolongation of standing time, which is caused by the water evaporation.

It can be clearly seen that the XRD patterns of these films become obvious with the prolongation of deposition time. The XRD pattern of iron substrates is indicated by the asterisk (∗), and the Ni–P alloy XRD patterns are shown by the red dashed line in Figure SI3 (Supporting Information). The fcc Ni (ICSD PDF No. 70-1849) diffraction angles of 44°, 51°, and 76° are shown in the figure, and the diffraction peak near 44° is overlapped with the diffraction peak produced by Fe substrate (110) crystal face. As shown in the figure, the diffraction peak near the diffraction angle of 44° changed to wider with the deposition time increased, which is due to the thickening of Ni–P deposits. From the XRD patterns, it is shown that the alloy films have been successfully deposited on the substrates.

XPS spectra analyses are conducted to probe which components are present in the films. The results are shown in Figure 4. As shown in the Ni spectrum (Figure 4a), most of element Ni corresponds to metallic Ni with a binding energy of 852.4 eV and the other element Ni to NiO with a binding energy of 853.7 eV. Both of electrochemical deposition and chemical deposition can reduce nickel ions into zero valence state of Ni. NiO is probably due to the oxidation of Ni by the oxygen in the air. As shown in the P spectrum (Figure 4b), there is a strong peak located at near 130 eV. This peak is attributed to the superposition of peaks of the P $2p_{3/2}$ and P $2p_{1/2}$ corresponding to chemical valence state of elemental phosphorus in the red phosphorus. In the process of depositing Ni and P, nickel ions are almost reduced by electrons at the surface of cathode. According to the previous report,[41] hypophosphite can generate elemental form of phosphorus

dx.doi.org/10.1021/am404590d | ACS Appl. Mater. Interfaces 2014, 6, 1053–1060

both by electrochemical deposition and chemical deposition. The elemental form of P is obtained by the two deposition methods. The peak near the 130 eV can not be used to identify the reaction of chemical deposition, however, that at 133.0 eV which corresponding to P 2p state of phosphite radicals ($H_2PO_3^-$) can certify the chemical deposition of nickel ions with hypophosphite. Obviously, the chemical reduction between hypophosphite and nickel ion[21,42] has occurred. The chemical reaction of the nickel ion in acid solutions can be expressed as:

$$H_2PO_2^- + Ni^{2+} + H_2O = H_2PO_3^- + Ni + 2H^+$$

So, the phosphite is the oxidation product of this chemical reducing reaction. This form of element P gives direct evidence for the occurrence of chemical deposition. Insets in Figure 4a and b show the XPS data of samples deposited for different deposition times, and they all show the similar binding energy.

Films deposited with various reducing agent content in solution also show a morphology evolution. When there is 0.01 M reducing agent in the solution (Figure 5a), the Ni−P film possesses a smooth surface composed with nanoscale particles but without microscale structure. And the microscale structure arises with further addition of reducing agent (Figure 5c and d). There are many mastoid-like structures in different growth stages (see Figure 5e and f). It is the evidence that these films are grown based on the progressive nucleation of Scharifker−Hills rule.[36,43] According to this rule, two diagnostic relationships can be used to determine whether the nucleation of the Ni−P patterned alloy films is instantaneous or progressive. If the nucleation is instantaneous, the clusters would be in the same size and relevant result has been published by Grujicic and co-workers.[44] There are large and small protrusions, which means the formation of new nuclei is faster than the growth of existing nuclei. The result is the progressive superposition of the currents of formation and growth of each nucleus. Figure 5e demonstrates an immature protrusion. This protrusion is composed of a crowd of nanoscale particles, making its surface rough. Figure 5f shows a mature protrusion, which is also composed of many nanoscale particles through careful observation. By the comparison of the two protrusions, the mature one's surface is smoother than that of the immature one. This phenomena can be explained by the theory on the unstable growth process.[33] The immature ones hide under the patterned films, and the diffusion layer is thick here, making the metal ions difficult diffusing into these protrutions surface. However, when the protrusions grow larger, they can stretch into the bulk solution, and the diffusion layer here is thin. According to the unstable growth theory, the thinner the diffusion layer becomes, the smaller the particles tend to appear.[33] The particles size on immature protrusions are large making the protrusions appear rough. On the contrary, the mature ones appear smooth.

3.2. Patterned Film Growth Mechanism. The growth mechanism of these patterned Ni−P alloy films could be explained by the "reducing−discharging" film growth process. "Reducing" process is the main driving force for the formation of nanoscale particles and "discharging" process induces the main film growth and formation of microscale structures. The schematic illustration of mechanism of patterned Ni−P ally film and pure Ni film are depicted in Figure 6.

When the deposition time is only 1 min, the nanoscale particles are formed mainly by the reduction of reducing agent NaH_2PO_2. The low particle density occurs because of the low concentration of reducing agent in the electrolyte and low reaction probability of nickel ions with reducing agents, and also the low activity of nickel ions on the smooth surface. After being deposited for 5 min, much more nanoscale particle clusters appear on the substrate. The nickel ions existing at the edges of nickel particles are more easily reduced by the "discharging" process of the cathode because the bigger the roughness is, the higher the current density is, making the nickel ions here more active. This explanation also can be illustrated/supported by the aggregation of the particles. There is another reason for the formation of particle morphology. The traditional Ni deposition process will not get the smooth film because deposits would be "burned" if the current density is too high. This phenomenon is very common in the field of electrochemical deposition. Based on these theories above, the ongoing deposition process would get more rough morphology. The relative smooth base plate is caused by the electrochemical deposition. The electrochemical deposition is the main source of the Ni−P alloy film growth. With the increase of the deposition time, the combination of "reducing−discharging" process results in the formation of the micro-nanoscale patterned film.

Furthermore, the pure Ni film growth mechanism is proposed for comparison with the Ni−P alloy film growth. The Ni film growth process is obviously different with the alloy film growth process, and the simplified diagram is also shown in Figure 6. The Ni film spread out of the substrate with no surface morphology feature. As deposition time goes on, the pure Ni film covers the whole substrate. At last, the Ni films fabricated by the pure electrochemical deposition are smooth and bright from the respective of real samples.

3.3. Wetting Behavior of the Ni−P Alloy Patterned Films. Water wetting/dewetting behaviors of these films just after their fabrication are tested as one of the many applications (Figure 7). The contact angle of films with water gradually increases, from about 105° when deposition time is 1 min to superhydrophobic 155° when deposition time is 60 min. As shown in the SEM images above, film morphologies vary from almost smooth surface with some dots distributing on the film to micro-nanostructures with the prolongation of deposition time. The surface profilometer test shows that these films roughness gradually increase (Figure 9). The increase of roughness and the formation of patterned micro-nanostructure morphology lead to the contact angle with water increase (Figures 7 and 8).

Smooth Ni−P films are fabricated by electrodeposition with H_3PO_3 in the electrolyte as controlled examples. The results are shown in Figure 9. The Ni−P smooth film shows hydrophilic property with contact angle of 46° compared with patterned Ni−P alloy films of 155°. Therefore, the superhydrophobicity of the patterned film is caused by the multiscale surface features. When a water droplet is brought in contact with the patterned film, it does not leave the syringe tip. That is to say, the droplet is repelled by these surfaces and cannot be replaced on the surface. The Ni−P patterned alloy film's contact angle hysteresis has been tested (Supporting Information Video 1). A water droplet freely falls on the superhydrophobic surface. The sample stage tilts and the advancing and receding contact angle is recorded when the droplet moves. The result shows that the contact angle hysteresis is less than 1°, which further shows the superhydrophobic characteristic of the patterned films.

After 3 months of sample preparation, contact angle measurement is performed again to test the contact angle

stability (Figure 10). The result shows that the starting contact angle is still as high as 155°, well maintaining its superhydrophobic property, compared with the contact angle shown in Figure 8. The variation of contact angle with time shown in Figure 10, from 155° to 150°, is very little, which is mainly caused by the water evaporation. The 10 min contact angle test here also shows the alloy film wetting behavior's stability contrast with some contact angle measurement where contact angle will change with time.

4. CONCLUSIONS

In summary, Ni−P alloy films with patterned morphology have been prepared by "reducing−discharging" process, the synergistic effect of electrochemical deposition and chemical deposition. These film morphologies change regularly along with the increase of deposition time. There appear many nanoscale particles, formed by chemical deposition, scattering at the surface of the smooth film surface, deposited mainly by electrochemical deposition, when deposition time is short. And then, particles become larger and more, and aggregate together forming cluster islands. With the deposition time increases, these islands occupy mostly area underneath the film. After 0.5 h deposition, the surface morphology exhibits some three-dimensional patterns slightly. The micro-nanostructural morphology forms after 1 h deposition. The phosphorus element valence states detected by XPS show the coexistence of elemental states corresponding to that of red phosphorus, and oxidation state to phosphite radicals, giving direct evidence for the co-occurrence of electrochemical deposition and chemical deposition. This methodology of synergistic effect of electrochemical deposition and chemical deposition to preparing patterned films is undergoing further study to expand to other metal systems.

■ ASSOCIATED CONTENT

Ⓢ Supporting Information

Pure Ni films SEM images and EDX spectrum, XRD spectrum of Ni−P alloy films (PDF). This material is available free of charge via the Internet at http://pubs.acs.org.

■ AUTHOR INFORMATION

Corresponding Authors

*(Z.Z.) E-mail: zzx1572000@aliyun.com.cn. Tel.: +86 057486685036. Fax:86057486685159.

*(X.W.) E-mail: xdwu@nimte.ac.cn.

Notes

The authors declare no competing financial interest.

■ ACKNOWLEDGMENTS

Projects 51105356 and 51335010 supported by National Nature Science Foundation of China. This material is also based upon work funded by Zhejiang Provincial Innovation Team (Grant No. 2011R50006) and Ningbo Municipal Innovation Team (Grant No. 2011B31023).

■ REFERENCES

(1) Zhang, L.; Wu, J.; Wang, Y.; Long, Y.; Zhao, N.; Xu, J. *J. Am. Chem. Soc.* **2012**, *134*, 9879−9881.
(2) Andreoli, E.; Annibaldi, V.; Rooney, D. A.; Liao, K.-S.; Alley, N. J.; Curran, S. A.; Breslin, C. B. *Electroanalysis* **2011**, *23*, 2164−2173.
(3) Fan, J.; Zhao, C.; Fan, L. *Acta Chim. Sin.* **2012**, 24−29.
(4) Wang, H.-L.; Li, W.; Jia, Q. X.; Akhadov, E. *Chem. Mater.* **2007**, *19*, 520−525.
(5) Crossland, E. J.; Noel, N.; Sivaram, V.; Leijtens, T.; Alexander-Webber, J. A.; Snaith, H. J. *Nature* **2013**, *495*, 215−9.
(6) Facchetti, A. *Nat. Mater.* **2013**, *12*, 598−600.
(7) McShane, C. M.; Choi, K.-S. *J. Am. Chem. Soc.* **2009**, *131*, 2561−2569.
(8) Barthlott, W.; Neinhuis, C. *Planta* **1997**, *202*, 1−8.
(9) Feng, L.; Zhang, Y.; Xi, J.; Zhu, Y.; wang, N.; Xia, F.; Jiang, L. *Langmuir* **2008**, *24*, 4114−4119.
(10) Menke, E. J.; Thompson, M. A.; Xiang, C.; Yang, L. C.; Penner, R. M. *Nat. Mater.* **2006**, *5*, 914−919.
(11) Nie, Z.; Kumacheva, E. *Nat. Mater.* **2008**, *7*, 277−290.
(12) Yu, H.-D.; Regulacio, M. D.; Ye, E.; Han, M.-Y. *Chem. Soc. Rev.* **2013**, *42*, 6006−6018.
(13) Claridge, S. A.; Liao, W.-S.; Thomas, J. C.; Zhao, Y.; Cao, H. H.; Cheunkar, S.; Serino, A. C.; Andrews, A. M.; Weiss, P. S. *Chem. Soc. Rev.* **2013**, *42*, 2725−2745.
(14) Lieber, C. M. *MRS Bull.* **2003**, *28*, 486−491.
(15) Cavallini, M.; Albonetti, C.; Biscarini, F. *Adv. Mater.* **2009**, *21*, 1043−1053.
(16) Pan, Z.; Dai, S.; Beach, D. B.; Lowndes, D. H. *Nano Lett.* **2003**, *3*, 1279−1284.
(17) Lopes, W. A.; Jaeger, H. M. *Nature* **2001**, *414*, 735−738.
(18) Wang, M.; Wudl, F. *J. Mater. Chem.* **2012**, *22*, 24297−24314.
(19) Pennelli, G.; Totaro, M.; Nannini, A. *ACS Nano* **2012**, *6*, 10727−10734.
(20) Bennett, C. W.; Kenny, H. C.; Dugliss, R. P. *J. Phys. Chem.* **1914**, *18*, 373−384.
(21) Brenner, A.; Riddell, G. E. *J. Res. Natl. Bur. Stand.* **1946**, *37*, 31−34.
(22) Siegfried, M. J.; Choi, K.-S. *Angew. Chem.* **2005**, *117*, 3282−3287.
(23) Siegfried, M. J.; Choi, K.-S. *J. Am. Chem. Soc.* **2006**, *128*, 10356−10357.
(24) Siegfried, M. J.; Choi, K.-S. *Angew. Chem., Int. Ed.* **2008**, *47*, 368−372.
(25) Shpaisman, N.; Givan, U.; Patolsky, F. *ACS Nano* **2010**, *4*, 1901−1906.
(26) Qiu, R.; Cha, H. G.; Noh, H. B.; Shim, Y. B.; Zhang, X. L.; Qiao, R.; Zhang, D.; Kim, Y. I.; Pal, U.; Kang, Y. S. *J. Phys. Chem. C* **2009**, *113*, 15891−15896.
(27) Qiu, R.; Zhang, X. L.; Qiao, R.; Li, Y.; Kim, Y. I.; Kang, Y. S. *Chem. Mater.* **2007**, *19*, 4174−4180.
(28) Li, G.-R.; Yao, C.-Z.; Lu, X.-H.; Zheng, F.-L.; Feng, Z.-P.; Yu, X.-L.; Su, C.-Y.; Tong, Y.-X. *Chem. Mater.* **2008**, *20*, 3306−3314.
(29) Monzon, L. M. A.; Rode, K.; Venkatesan, M.; Coey, J. M. D. *Chem. Mater.* **2012**, *24*, 3878−3885.
(30) Xu, P.; Akhadov, E.; Wang, L.; Wang, H.-L. *Chem. Commun.* **2011**, *47*, 10764−10766.
(31) Mullins, W. W.; Sekerka, R. F. *J. Appl. Phys.* **1964**, *35*, 444−451.
(32) Aogaki, R.; Makino, T. *Electrochim. Acta* **1981**, *26*, 1509−1517.
(33) Aogaki, R.; Kitazawa, K.; Kose, Y.; Fueki, K. *Electrochim. Acta* **1980**, *25*, 965−972.
(34) Haghdoost, A.; Pitchumani, R. *Langmuir* **2013**, DOI: 10.1021/la403509d.
(35) Shirtcliffe, N. J.; McHale, G.; Newton, M. I.; Perry, C. C. *Langmuir* **2005**, *21*, 937−943.
(36) Andreoli, E.; Annibaldi, V.; Rooney, D. A.; Breslin, C. B. *J. Phys. Chem. C* **2011**, *115*, 20076−20083.
(37) Andreoli, E.; Rooney, D. A.; Redington, W.; Gunning, R.; Breslin, C. B. *J. Phys. Chem. C* **2011**, *115*, 8725−8734.
(38) Yu, Q.; Zeng, Z.; Zhao, W.; Li, H.; Wu, X.; Xue, Q. *Chem. Commun.* **2013**, *49*, 2424−2426.
(39) Daly, B. P.; Barry, F. J. *Int. Mater. Rev.* **2003**, *48*, 326−338.
(40) Peeters, P.; Hoorn, G. v. d.; Daenen, T.; Kurowski, A.; Staikov, G. *Electrochim. Acta* **2001**, *47*, 161−169.
(41) Haseeb, A. S. M. A.; Chakraborty, P.; Ahmed, I.; Caccavale, F.; Bertoncello, R. *Thin Solid Films* **1996**, *283*, 140−144.
(42) Bremner, J. G. M. *Nature* **1948**, *162*, 183−184.
(43) Scharifker, B.; Hills, G. *Electrochim. Acta* **1983**, *28*, 879−889.

(44) Grujicic, D.; Pesic, B. *Electrochim. Acta* **2006**, *51*, 2678−2690.